NBP IAV increases when we use the semiannual drivers, which suggests the importance of accounting for time lags and the "period of climatic influence" of P variations (*12*), but P correlations with NBP IAV are still weaker than T correlations with NBP IAV (Fig. 4C).

Our analysis provides evidence that semi-arid ecosystems, largely occupying low latitudes, have dominated the IAV and trend of the global land carbon sink over recent decades. Semi-arid regions have been the subject of relatively few targeted studies that place their importance in a global context. Our findings indicate that semi-arid regions and their ecosystems merit increased attention as a key to understanding and predicting interannual to decadal variations in the global carbon cycle.

REFERENCES AND NOTES

1. C. Le Quéré *et al.*, *Earth Syst. Sci. Data* **6**, 235–263 (2014).
2. C. D. Keeling, T. P. Whorf, M. Wahlen, J. van der Plichtt, *Nature* **375**, 666–670 (1995).
3. C. Le Quéré *et al.*, *Nat. Geosci.* **2**, 831–836 (2009).
4. A. Ahlström, G. Schurgers, A. Arneth, B. Smith, *Environ. Res. Lett.* **7**, 044008 (2012).
5. P. Friedlingstein *et al.*, *J. Clim.* **19**, 3337–3353 (2006).
6. A. D. McGuire *et al.*, *Glob. Biogeochem. Cycles* **15**, 183–206 (2001).
7. S. Schaphoff *et al.*, *Clim. Change* **74**, 97–122 (2006).
8. S. Sitch *et al.*, *Glob. Change Biol.* **14**, 2015–2039 (2008).
9. Y. Pan *et al.*, *Science* **333**, 988–993 (2011).
10. A. Ahlström, P. A. Miller, B. Smith, *Geophys. Res. Lett.* **39**, L15403 (2012).
11. B. Smith, I. C. Prentice, M. T. Sykes, *Glob. Ecol. Biogeogr.* **10**, 621–637 (2001).
12. See supplementary materials on *Science* Online.
13. I. Harris, P. D. Jones, T. J. Osborn, D. H. Lister, *Int. J. Climatol.* **34**, 623–642 (2014).
14. G. Hurtt *et al.*, *Clim. Change* **109**, 117–161 (2011).
15. S. Sitch *et al.*, *Biogeosciences* **12**, 653–679 (2015).
16. M. A. Friedl *et al.*, *Remote Sens. Environ.* **114**, 168–182 (2010).
17. N. Andela, Y. Y. Liu, A. I. J. M. van Dijk, R. A. M. de Jeu, T. R. McVicar, *Biogeosciences* **10**, 6657–6676 (2013).
18. R. J. Donohue, T. R. McVicar, M. L. Roderick, *Glob. Change Biol.* **15**, 1025–1039 (2009).
19. R. Fensholt *et al.*, *Remote Sens. Environ.* **121**, 144–158 (2012).
20. B. Poulter *et al.*, *Nature* **509**, 600–603 (2014).
21. M. Jung *et al.*, *J. Geophys. Res.* **16**, G00J07 (2011).
22. J. Zscheischler *et al.*, *Environ. Res. Lett.* **9**, 035001 (2014).
23. M. Reichstein *et al.*, *Nature* **500**, 287–295 (2013).
24. M. D. Smith, *J. Ecol.* **99**, 656–663 (2011).
25. W. Cai *et al.*, *Nat. Clim. Change* **4**, 111–116 (2014).
26. K. E. Trenberth *et al.*, *Nat. Clim. Change* **4**, 17–22 (2014).
27. A. Dai, *Nat. Clim. Change* **3**, 52–58 (2013).
28. X. Wang *et al.*, *Nature* **506**, 212–215 (2014).
29. W. Wang *et al.*, *Proc. Natl. Acad. Sci. U.S.A.* **110**, 13061–13066 (2013).
30. P. M. Cox *et al.*, *Nature* **494**, 341–344 (2013).
31. K. Wolter, M. S. Timlin, in *Proceedings of the 17th Climate Diagnostics Workshop* (University of Oklahoma, Norman, OK, 1993), pp. 52–57; www.esrl.noaa.gov/psd/enso/mei/WT1.pdf.
32. K. Wolter, M. S. Timlin, *Weather* **53**, 315–324 (1998).

ACKNOWLEDGMENTS

This paper is dedicated to the memory of Michael Robin Raupach (1950–2015), whose scientific integrity and novel contributions leave a long-lasting legacy in the field of carbon cycle sciences. The MODIS MOD12C1 land cover product was obtained through the online Data Pool at the NASA Land Processes Distributed Active Archive Center (LP DAAC), USGS/Earth Resources Observation and Science (EROS) Center, Sioux Falls, South Dakota (https://lpdaac.usgs.gov/data_access). Supported by the Royal Physiographic Society in Lund (Birgit and Hellmuth Hertz Foundation), Swedish Research Council grant 637-2014-6895, and the Mistra-SWECIA program (A. Ahlström); EC FP7 grant LUC4C (603542) (A. Arneth); OCE Distinguished Visiting Scientist to the CSIRO Ocean and Atmosphere Flagship, Canberra (B.S.); EC FP7 grant EMBRACE (282672) (A. Arneth, M.R., and B.D.S.); the Australian Climate Change Science Program (J.G.C.); NSF grant AGS 12-43071, U.S. Department of Energy grant DE-SC0006706, and NASA LCLUC program grant NNX14AD94G (A.K.J.); the Environmental Research and Technology Development Fund (S-10) of the Ministry of Environment of Japan (E.K.); CSIRO strategic research funds (Y.P.W.); and NOAA grants NA10OAR4310248 and NA09NES4400006 and NSF grant AGS-1129088 (N.Z.). This study is a contribution to the Lund Centre for Studies of Carbon Cycle and Climate Interactions (LUCCI) and the strategic research areas MERGE and BECC.

SUPPLEMENTARY MATERIALS

www.sciencemag.org/content/348/6237/895/suppl/DC1
Materials and Methods
Figs. S1 to S12
References (*33*–*56*)

26 October 2014; accepted 24 April 2015
10.1126/science.aaa1668

GLACIER MASS LOSS

Dynamic thinning of glaciers on the Southern Antarctic Peninsula

B. Wouters,[1]* A. Martin-Español,[1] V. Helm,[2] T. Flament,[3] J. M. van Wessem,[4] S. R. M. Ligtenberg,[4] M. R. van den Broeke,[4] J. L. Bamber[1]

Growing evidence has demonstrated the importance of ice shelf buttressing on the inland grounded ice, especially if it is resting on bedrock below sea level. Much of the Southern Antarctic Peninsula satisfies this condition and also possesses a bed slope that deepens inland. Such ice sheet geometry is potentially unstable. We use satellite altimetry and gravity observations to show that a major portion of the region has, since 2009, destabilized. Ice mass loss of the marine-terminating glaciers has rapidly accelerated from close to balance in the 2000s to a sustained rate of –56 ± 8 gigatons per year, constituting a major fraction of Antarctica's contribution to rising sea level. The widespread, simultaneous nature of the acceleration, in the absence of a persistent atmospheric forcing, points to an oceanic driving mechanism.

Ice shelves have been identified as sensitive indicators of climate change (*1*). Their retreat along the coast of the Northern Antarctic Peninsula has been noted over recent decades (*2*) and associated with a sudden and prolonged increase in discharge of the inland grounded ice (*3*–*5*), especially for those glaciers overlying deep troughs (*6*). The potential future contribution to sea-level rise of these glaciers relatively modest because their catchments are small compared with those further south (*7*). The Southern Antarctic Peninsula (SAP), including Palmer Land and the Bellinghausen Coast, rests on bedrock below sea level with a retrograde slope (deeper inland) (*8*), which is believed to be an inherently unstable configuration (*9*), permitting rapid grounding line retreat and mass loss to the ocean. Recent modeling results suggest that this marine ice sheet instability may have already been initiated for part of West Antarctica (*10*, *11*).

The SAP is home to a number of fast flowing, marine terminating glaciers, many of which are still unnamed. Laser [ICESat, 2003–2009 (*12*)] and radar [Envisat, 2003– 2010 (*13*)] altimetry identified moderate surface-lowering concentrated within a narrow strip along the coast, in particular near the grounding line of the Ferrigno Ice Stream (*14*), contrasted by widespread thickening further inland. Observations from the Gravity Recovery and Climate Experiment (GRACE) mission show that these opposing signals compensated each other, resulting in a near-zero mass balance for 2002–2010 (*15*).

The Cryosat-2 satellite, launched in April 2010, provides elevation measurements of land and sea ice at a high spatial resolution up to a latitude of 88°. In contrast to conventional altimetry missions such as Envisat, Cryosat-2's dual antenna and Doppler processing results in improved resolution and geolocation of the elevation measurement (*16*). Because of the long satellite repeat period of 369 days, it has a dense track spacing in our region of interest, which is a major advantage compared with the roughly 10-times-coarser ICESat track spacing. Two recent studies using Cryosat-2 data observed thinning along the coast of the Bellinghausen Sea (*17*, *18*). Such elevation changes may result from either a decrease in surface mass balance (SMB) (accumulation minus ablation), compaction of the firn column, or an increase in the ice flow speed (also termed dynamic thinning). Both studies attributed the surface-lowering to interannual changes in SMB, based on the strong accumulation variability observed in the Gomez ice core (70.36°W, 73.59°S) (*18*, *19*). Here, we take SMB and firn compaction into account and show that the

[1]Bristol Glaciology Centre, University of Bristol, Bristol, UK. [2]Alfred-Wegener-Institut Helmholtz-Zentrum für Polar- und Meeresforschung, Bremerhaven, Germany. [3]Laboratoire d'Etudes en Géophysique et Océanographie Spatiales, Toulouse, France. [4]Institute for Marine and Atmospheric Research, Utrecht University, Netherlands.
*Corresponding author. E-mail: bert.wouters@bristol.ac.uk

signal is due to pronounced glacier dynamic ice loss instead.

We used a pseudo-repeat track method to derive elevation changes from the Cryosat-2 measurements (July 2010 to April 2014), which makes optimal use of the available observations (*20*), allows us to observe small-scale features such as the changes of the narrow Nikitin Glacier (Fig. 1B), and compares well with trends derived from high-accuracy, high-resolution airborne laser altimetry campaigns (fig. S1). Strong negative elevation trends are found along a roughly 750-km western coastal transect between the catchments of the Jensen Nunataks and the Wesnet and Williams Ice Stream (regions denoted in Fig. 1A), which are mainly localized in areas of fast glacier flow (fig. S2 for comparison). The average observed elevation rate in our area of interest [basins 23 and 24 as defined in (*21*) and used in the ice sheet mass balance inter-comparison exercise (IMBIE) study (*22*)] equals −0.42 m/year, with catchment averages as negative as −1.15 m/year for the Fox Ice Stream (table S1). Locally, near the grouding line, thinning rates in this catchment reach values down to −4 m/year. Thinning is also pronounced in the English Coast region, with rates close to the grounding line of −2 m/year or more occurring for several of the glaciers.

Integrated over the entire region (174,101 km^2), volume losses total −72 ± 10 km^3/year (July 2010 to April 2014) (table S2). Part of this signal is due to changes in the air content of the firn column, which is caused by variability in temperature and accumulation (and thus no associated change in mass) alongside variations in SMB. To correct for these two effects, we used a firn densification model (*23*) driven by a regional climate model (*24*). The variations in SMB and firn densification rate are more widespread—and not tied to fast flowing narrow glacier areas—and are an order of magnitude too small to explain the observed elevation changes (fig. S3). After correcting the altimetry rates with the firn densification model, the link between the surface-lowering and fast flowing ice becomes even more evident, with the majority of negative trends occurring between the coastline and the 50-m/year velocity contour (fig. S4B).

The firn model prescribes a volume change of −15 ± 3 km^3/year to surface processes. Attributing the remainder to ice dynamics (at a density of ρ_{ice} = 917 kg/m^3), and adding back the modeled SMB mass anomalies (fig. S5), yields a total mass loss of −59 ± 10 gigatons (Gt)/year. Repeating this approach for elevation rates obtained from combined ICESat/Envisat observations during 2003–2009 (*20*) shows a contrasting picture, with a near-balance during 2003–2009 (3 ± 22 Gt/year), with slightly more positive values at the beginning of the observations (2003–2005, 15 ± 26 Gt/year) compared with the end (2007–2009, −10 ± 15 Gt/year). This suggests a remarkable rate of acceleration in dynamic mass loss since about 2009 that must have been near-simultaneous across multiple basins and glaciers.

The GRACE satellites measure changes in mass distribution at, and beneath, the surface (*25*). Because these gravimetric observations are insensitive to the underlying processes causing the mass redistribution (in this case, either ice dynamics or SMB, or a combination), they offer an independent method with which to validate the altimetric observations. The GRACE data shows an increase in mass loss in our region of interest (fig. S6) and are consistent with the ICESat/Envisat and Cryosat-2 observations within uncertainties at all time intervals (table S3). The region was in approximate balance for 2003–2009 (−11 ± 5 Gt/year) (Fig. 2), with first signs of mass loss appearing around 2008, but these are at least partially caused by a temporal reduction in SMB. Rapid dynamic ice loss started in 2009 and has continued unabated since (−52 ± 14 Gt/year for July 2010 to April 2014). Although the post-2009 time series is still modulated by SMB variability (for example, the short-lived down- and upward event in 2010) (Fig. 2), the current mass loss lies clearly outside the range of variability observed in the modeled cumulative SMB for 1979 to present (10 Gt). GRACE trends are sensitive to mass redistribution related to glacial isostatic adjustment, but this signal is negligible in the region (2 ± 1 Gt/year) and because it is constant over these time scales, the sudden increase in mass loss cannot be explained

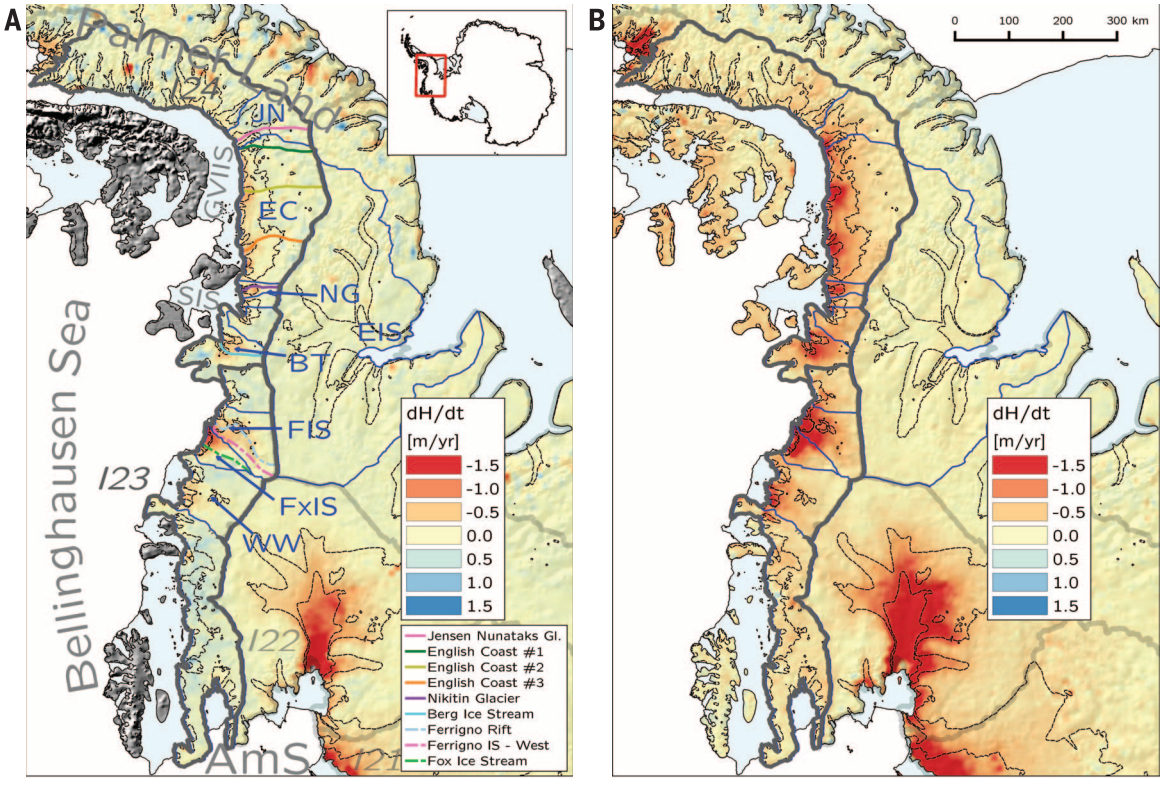

Fig. 1. Elevation rates in the Bellinghausen Sea Sector. (**A**) Envisat/ICESat (2003–2009). (**B**) Cryosat-2 (2010–2014). No correction for elevation changes due to surface processes was applied (results with this correction are provided in fig. S4). Where available, the 50- and 250-m/year velocity contours are plotted (*36*). (Inset) The location of our area of interest. The elevation rates profiles of Fig. 3 are indicated by colored lines. Glaciers basins are outlined in blue (*37*); JN, Jensen Nunataks; EC, English Coast; NG, Nitikin Glacier; BT, Berg & Thompson Ice Stream; FIS, Ferrigno Ice Stream; FxIS, Fox Ice Stream; WW, Wesnet & Williams Ice Stream; EIS, Evans Ice Stream (names of other basins are available in fig. S4). IMBIE basins are shown in gray (I23 and I24) and pale gray. Ice shelves are plotted in light blue; grounding lines are based on (*30*). GVIIS, George VI Ice Shelf; SIS, Stange Ice Shelf; AmS, Amundsen Sea.

by this source. Combining the Cryosat-2– and GRACE-derived rates yields an error-weighted mean mass loss of 56 ± 8 Gt/year for July 2010 to April 2014.

To further investigate the temporal and spatial evolution of the dynamic thinning, we sampled surface elevation rates along a number of profiles of glaciers displaying pronounced surface-lowering (locations are shown in Fig. 1A and fig. S2). As reported in earlier studies (*12*–*14*), Ferrigno Ice Stream showed thinning rates of up to 1 m/year, along the deep, subglacial rift system extending inland (*14*) during the ICESat and Envisat observation periods. No significant increase in thinning took place near the grounding line between 2003–2005 and 2007–2009, but elevation rates further upstream were slightly more negative during the latter period. In recent years, thinning near the grounding line has more than doubled and propagated ~100 km inland, which is characteristic of a dynamic thinning signal (*26*). Even larger changes are observed along the western tributary of the ice stream (Fig. 3) and the Fox Ice Stream, where locally, surface-lowering of roughly –4 m/year is now occurring at the glacier fronts, and ice drawdown stretches 75 to 100 km inland.

Further to the east, the unnamed glacier in the Jensen Nunataks region and unnamed glacier #1 in the English Coast basin were in near-balance up to 2009, whereas English Coast unnamed glacier #2 showed thinning (~1 m/year) at its front. During 2010–2014, all three glaciers showed negative elevations rates exceeding –2 m/year at their grounding lines, which become gradually less pronounced further upstream. At all nine glacier profiles surveyed, elevation rates were consistently more negative during the latter period.

In terms of larger-scale spatial variability, glacier-thinning is restricted to the western side of the southwest Peninsula. For instance, the Berg Ice Stream shows thinning up to the Peninsula's divide (–0.5 ± 0.1 m/year) (Fig. 3), with barely detectable trends on the ice on the eastern side of the divide feeding into the the Evans Ice Stream. The basin of this neighboring ice stream (118 300km^2) (Fig. 1) has been in near balance during the entire study period, with a total mass change of only 8 ± 20, 3 ± 12, and –3 ± 13 Gt/year for 2003–2005, 2007–2009, and 2010–2014, respectively.

The widespread and simultaneous speed-up of the southwest Antarctic Peninsula marine-terminating glaciers, in the absence of persistent changes in SMB in the region, points to ocean processes as the driving mechanism. Near the continental margin of the Bellinghausen Sea, warm Circumpolar Deep Water (CDW) slopes upward toward shallower depths, facilitating episodic but persistent intrusion of CDW onto the continental shelf (*27*, *28*). These water masses have direct access to the glacier fronts of the Ferrigno and Fox Ice Streams, via the Belgica Trough and Eltanin Bay (fig. S2) (*14*). The eastern glaciers of the SAP flow into the Stange ice shelf and George VI ice shelf (GVIIS), the second largest ice shelf on the Antarctic Peninsula, and particularly vulnerable to intrusion of CDW (*2*, *29*). CDW is channeled below the GVIIS through the George VI Sound, resulting in basal melt of several meters per year (*29*–*31*), which is not fully compensated by surface mass accumulation and glacier inflow (*30*, *31*). As a result, the GVIIS has been thinning during the past few decades, with recent rates on the order of –1.5 m/year near the grounding lines of glaciers feeding the southeastern flank of the GVIIS (*32*). Simultaneously, increased rifting has been reported, rendering parts of the GVIIS structurally weak, combined with a retreat of the southern ice shelf front (*29*). Using LANDSAT imagery, we estimate a loss of about 495 km^2 in the period 2000–2013, with 265 km^2 occurring in the period 2010–2013 (fig. S7) (*20*).

The recent increase in thinning of the glaciers in our region of interest coincides with a record high in in situ temperatures measured at the bed of the Bellinghausen Sea in the 2010s, which is attributed to shoaling and warming of offshore CDW (*28*). This, combined with the observed thinning and weakening of GVIIS, shows strong similarities with the recent changes observed in the Amundsen Sea sector. There, increased subglacial melt from the intrusion of CDW into the ice shelf cavities lead to thinning of the shelves, and a sustained speed-up and thinning of the feeding glaciers (*33*). Depending on the local bathymetry and subglacial topography (*34*), glacier dynamics may be strongly coupled to the evolution of the seaward ice shelf, which provides a buttressing force on the glaciers' outflow. Both models and observations suggest that a decrease in back stress of a thinning ice shelf will lead to increased ice flux and inland retreat of the grounding line (*5*, *9*, *12*, *26*, *33*). Under the right conditions (a deep trough or submarine glacier bed and/or low basal shear stress), the glacier's dynamic response may extend far upstream (*26*), which is in agreement with our observations (Fig. 3). Although estimates of grounding zone locations in our region of interest are scarce, a grounding zone retreat has indeed been observed for some of the southern glaciers feeding into the GVIIS (*29*).

Dynamic thinning may be further promoted if the glacier is grounded below sea level on a bed with retrograde slope (*9*), as seen in the Amundsen Sea sector. Along the Bellinghausen Coast, such conditions are present at some of the glaciers showing the most pronounced thinning (fig. S2). The best documented example is the Ferrigno Rift (*14*), but the Nikitin Glacier and the unnamed glaciers of the English Coast show a similar configuration. The bedrock-deepening does not extend as far inland as observed in the Amundsen Sea Sector, but a large part of this region was inferred to be vulnerable to marine instability (*8*). Even if the forcing causing the observed thinning were to cease, dynamic thinning in the region will continue until the glaciers reach a new equilibrium

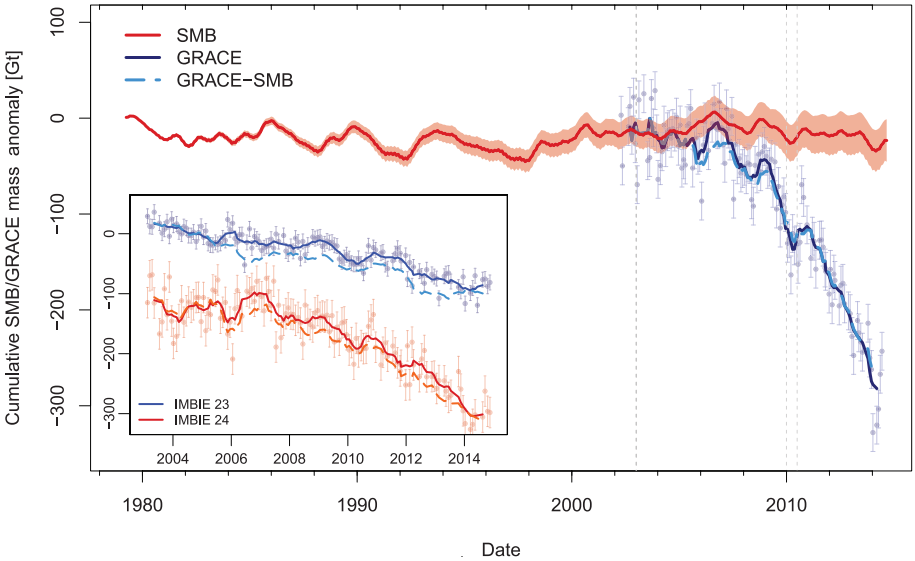

Fig. 2. Mass variations for the sum of basins 23 and 24, as observed by GRACE and modeled by RACMO2.3. Basins 23 and 24 are defined in (*21*, *22*). The faint blue dots are the monthly GRACE anomalies with 1σ error bars (*20*), and the thick blue line shows the anomalies with a 7-month running average applied so as to reduce noise. Cumulative SMB anomalies from RACMO2.3 are shown in red, with the light red area indicating the 1σ spread in an ensemble obtained by varying the baseline period (*20*). The dashed light blue line shows the estimated dynamic mass loss (GRACE minus SMB). The vertical dashed lines indicate January 2003, December 2009, and July 2010, the start and ending of the different altimetry observations. (Inset) The GRACE time series for the individual basins 23 (blue) and 24 (red), before (full lines) and after (dashed lines) applying the SMB correction.

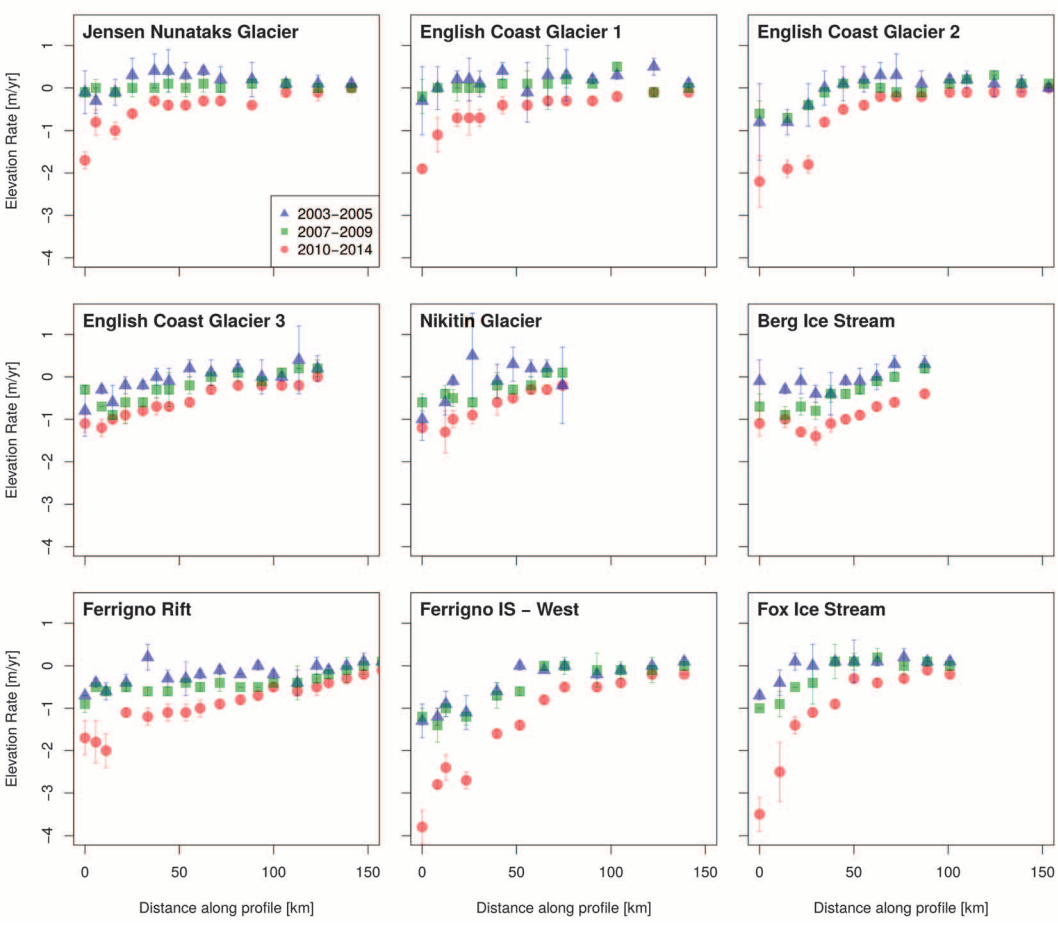

Fig. 3. Surface ice elevation rates along the profiles shown in Fig. 1, for 2003–2005, 2007–2009, and 2010–2014. 2003–2005, blue triangles; 2007–2009, green squares; 2010–2014, red circles. The altimetry observations have been corrected for surface processes, and the uncertainty bars are based on the root-square sum of the uncertainties in the altimetry data and the firn model.

state. The present losses of −56 ± 8 Gt/year are more than half of the mass loss in the Amundsen Sea Embayment [−80 to −110 Gt/year, depending on the period (*35*); IMBIE basins 21 and 22]. The Bellinghausen Coast glaciers currently add ~0.16 mm/year to global mean sea level and therefore constitute a major fraction of Antarctica's total oceanic contribution. The thinning and weakening of George VI, and other ice shelves along the western coast of the Peninsula (*32*), is most likely due to shoaling of relatively warm CDW onto the continental shelf (*12*, *28*). The intrusion of CDW will also lead to enhanced basal melting at the grounding line, resulting in steepening of the near-coast ice margin and therefore faster glacier flow. We conclude that these processes have resulted in the destabilization of the inland ice, resulting in a large and sustained mass loss to the ocean.

REFERENCES AND NOTES

1. D. G. Vaughan, C. S. M. Doake, *Nature* **379**, 328–331 (1996).
2. A. J. Cook, D. G. Vaughan, *Cryosphere* **4**, 77–98 (2010).
3. H. Rott, W. Rack, P. Skvarca, H. de Angelis, *Ann. Glaciol.* **34**, 277–282 (2002).
4. H. De Angelis, P. Skvarca, *Science* **299**, 1560–1562 (2003).
5. T. A. Scambos *et al.*, *Cryosphere* **8**, 2135–2145 (2014).
6. M. Rebesco *et al.*, *Science* **345**, 1354–1358 (2014).
7. M. Huss, D. Farinotti, *Cryosphere* **8**, 1261–1273 (2014).
8. J. L. Bamber, R. E. M. Riva, B. L. A. Vermeersen, A. M. LeBrocq, *Science* **324**, 901–903 (2009).
9. C. Schoof, *J. Geophys. Res.* **112** (F3), 3 (2007).
10. L. Favier *et al.*, *Nature Climate Change* **4**, 117–121 (2014).
11. I. Joughin, B. E. Smith, B. Medley, *Science* **344**, 735–738 (2014).
12. H. D. Pritchard *et al.*, *Nature* **484**, 502–505 (2012).
13. T. Flament, F. Rémy, *J. Glaciol.* **58**, 830–840 (2012).
14. R. G. Bingham *et al.*, *Nature* **487**, 468–471 (2012).
15. M. A. King *et al.*, *Nature* **491**, 586–589 (2012).
16. D. J. Wingham *et al.*, *Adv. Space Res.* **37**, 841–871 (2006).
17. M. McMillan *et al.*, *Geophys. Res. Lett.* **41**, 3899–3905 (2014).
18. V. Helm, A. Humbert, H. Miller, *Cryosphere* **8**, 1539–1559 (2014).
19. E. R. Thomas, G. J. Marshall, J. R. McConnell, *Geophys. Res. Lett.* **35**, 1706 (2008).
20. Materials and methods are available as supplementary materials on *Science* Online.
21. H. Zwally, M. B. Giovinetto, M. A. Beckley, J. L. Saba, *Antarctic and Greenland Drainage Systems* (GSF Cryospheric Sciences Laboratory, Greenbelt, MD, 2012).
22. A. Shepherd *et al.*, *Science* **338**, 1183–1189 (2012).
23. S. R. M. Ligtenberg, M. M. Helsen, M. R. van den Broeke, *Cryosphere* **5**, 809–819 (2011).
24. J. M. van Wessem *et al.*, *J. Glaciol.* **60**, 761–770 (2014).
25. B. Tapley, S. Bettadpur, M. Watkins, C. Reigber, *Geophys. Res. Lett.* **31**, L09607 (2004).
26. T. K. Dupont, R. B. Alley, *Geophys. Res. Lett.* **32**, 4503 (2005).
27. D. Holland, R. Thomas, B. de Young, M. Ribergaard, B. Lyberth, *Nat. Geosci.* **1**, 659–664 (2008).
28. S. Schmidtko, K. J. Heywood, A. F. Thompson, S. Aoki, *Science* **346**, 1227–1231 (2014).
29. T. O. Holt, N. F. Glasser, D. J. Quincey, M. R. Siegfried, *Cryosphere* **7**, 797–816 (2013).
30. M. A. Depoorter *et al.*, *Nature* **502**, 89–92 (2013).
31. E. Rignot, S. Jacobs, J. Mouginot, B. Scheuchl, *Science* **341**, 266–270 (2013).
32. F. S. Paolo, H. A. Fricker, L. Padman, *Science* **26**, (2015).
33. J. Mouginot, E. Rignot, B. Scheuchl, *Geophys. Res. Lett.* **41**, 1576–1584 (2014).
34. P. Dutrieux *et al.*, *Science* **343**, 174–178 (2014).
35. T. C. Sutterley *et al.*, *Geophys. Res. Lett.* **41**, 8421–8428 (2014).
36. E. Rignot, J. Mouginot, B. Scheuchl, *Science* **333**, 1427–1430 (2011).
37. The Scientific Committee on Antarctic Research, *SCAR Antarctic Digital Database*; available at www.add.scar.org, accessed 26 March 2015.

ACKNOWLEDGMENTS

B.W. and J.L.B. jointly conceived the study, interpreted the results, and wrote the article. B.W. processed the GRACE and Cryosat-2 L2 data. A.M.-E. combined the ICESat-Envisat elevation rates and derived the GVIIS front positions. V.H. developed the Cryosat-2 retracker and processed the L1B data. T.F. processed the Envisat data. J.M.v.W., S.R.M.L., and M.R.v.d.B. developed and ran the SMB and firn model. All authors commented on the manuscript. We thank J. Wahr and G. A for their help with the Glacial Isostatic Adjustment correction and elastic loading. G. Moholdt and A. Gardner are acknowledged for the fruitful discussions on altimetry. B.W. is funded by a Marie Curie International Outgoing Fellowship within the 7th European Community Framework Programme (FP7-PEOPLE-2011-IOF-301260). J.L.B. and A.M.-E. were supported by Natural Environment

Research Council grant NE/I027401/1. J.L.B., B.W., and A.M-E. also acknowledge support through European Space Agency contract 4000107393/12/I-NB, "REGINA." V.H. was supported by the German Ministry of Economics and Technology (grant 50EE1331). J.M.v.W., S.R.M.L., and M.R.v.d.B. acknowledge support from the Netherlands Polar Program of the Netherlands Organization for Scientific Research, section Earth and Life Sciences (NWO/ALW/NPP). The data sets used in this study can be found at http://pangaea.de.

SUPPLEMENTARY MATERIALS
www.sciencemag.org/content/348/6237/899/suppl/DC1
Materials and Methods
Figs. S1 to S9
Tables S1 to S4
References (*38*–*78*)

26 December 2014; accepted 28 April 2015
10.1126/science.aaa5727

SANITATION SUBSIDIES

Encouraging sanitation investment in the developing world: A cluster-randomized trial

Raymond Guiteras,[1] James Levinsohn,[2] Ahmed Mushfiq Mobarak[2]*

Poor sanitation contributes to morbidity and mortality in the developing world, but there is disagreement on what policies can increase sanitation coverage. To measure the effects of alternative policies on investment in hygienic latrines, we assigned 380 communities in rural Bangladesh to different marketing treatments—community motivation and information; subsidies; a supply-side market access intervention; and a control—in a cluster-randomized trial. Community motivation alone did not increase hygienic latrine ownership (+1.6 percentage points, $P = 0.43$), nor did the supply-side intervention (+0.3 percentage points, $P = 0.90$). Subsidies to the majority of the landless poor increased ownership among subsidized households (+22.0 percentage points, $P < 0.001$) and their unsubsidized neighbors (+8.5 percentage points, $P = 0.001$), which suggests that investment decisions are interlinked across neighbors. Subsidies also reduced open defecation by 14 percentage points ($P < 0.001$).

One billion people, or about 15% of the world's population, currently practice open defecation (OD), and another 1.5 billion do not have access to improved sanitation (*1*). Despite the existence of simple, effective solutions such as pour-flush latrines, poor sanitation causes 280,000 deaths per year (*2*) and may contribute to serious health problems such as stunting or tropical enteropathy (*3*–*5*).

The issue has attracted attention and resources from governments and development institutions. In 2012, the United Nations Children's Fund (UNICEF) spent USD 380 million on programs focused on water, sanitation, and hygiene for children (*1*). The World Bank's Water and Sanitation Program plans to direct USD 200 million in government and private funds to improve sanitation for 50 million people during the 2011–2015 period (*6*). In India, where over half the population practices open defecation (*7*), Prime Minister Narendra Modi declared "toilets first, temples later" during a 2013 speech and pledged to eliminate OD by 2019 (*8*–*10*).

However, disagreement remains over how best to increase sanitation coverage. Policymakers must allocate scarce resources among strategies such as demand generation (e.g., information campaigns, behavior change programming), direct provision of toilets to schools or households, or subsidizing consumers (*11*). Subsidies are particularly controversial, with practitioners concerned that subsidies may undermine intrinsic motivation or cause dependency (*12*, *13*). For example, the Government of India's Total Sanitation Campaign (TSC) used the rhetoric of "community-led," "people-centred," and "demand driven" to build one toilet for every 10 rural residents between 2001 and 2011 (*14*), but critics argue that the program as implemented was "infrastructure-centred" and "supply-led" (*15*). Recent studies of TSC find modest impacts on sanitation coverage and OD (*16*, *17*).

At the root of this disagreement is uncertainty about the reasons for low coverage. If the major constraints are poverty and the collective action problem posed by negative health externalities, then economic theory suggests that subsidies are necessary. If the key constraints are lack of information about the benefits of sanitation and the absence of strong community norms against OD, then programs such as Community-Led Total Sanitation (CLTS), which seek to change norms and create social pressure, could be sufficient without subsidies. Even when households are willing to pay for hygienic latrines, supply failures such as lack of access to markets where toilet components are sold, or lack of information about quality or installation methods, may impede adoption (*18*).

We measured the effects of alternative policies on investment in hygienic latrines using a cluster-randomized trial in 380 rural communities (18,254 households in 107 villages) in the Tanore district of northwest Bangladesh. Although sanitation coverage has increased markedly in rural Bangladesh in recent decades (*1*), progress in Tanore, located in the poorest region of the country, has been slower. At baseline, 31% of households reported that their primary defecation site was either no latrine (OD) or an unimproved latrine, and only 50% had regular access to a hygienic latrine. The intervention was conducted in 2012, and we collected follow-up data in 2013 (fig. S1).

We randomized communities to different treatments: a community motivation and health information campaign, called the Latrine Promotion Program (LPP); motivation and health information combined with subsidies for the purchase of hygienic latrines; a supply-side market access intervention linking villagers with suppliers and providing information on latrine quality and availability; and a control group receiving no interventions (*19*).

LPP was a multiday, neighborhood-level exercise to raise awareness of the problems caused by poor sanitation and to motivate the community to increase coverage of hygienic latrines. The design of LPP follows that of CLTS, an information and motivation intervention that has been implemented in over 60 countries worldwide (*20*). The nongovernmental organizations that implemented this project, WaterAid Bangladesh and Village Education Resource Center (VERC), were instrumental in the creation of CLTS (*13*). The design of LPP conformed closely to the principles of CLTS, although LPP differed in emphasizing the importance of hygienic latrines, rather than simply ending OD.

In villages assigned to the "subsidy" treatment, households in the bottom three-quarters of the wealth distribution were eligible to participate in a public lottery awarding subsidy vouchers. These vouchers provided a 75% discount on the components of any of three models of latrine, priced (after subsidy) USD 5.5, USD 6.5, and USD 12. Households were responsible for delivery and installation costs of USD 7 to 10. To study the extent of demand spillovers across neighbors, we randomized the share of lottery winners at the neighborhood level into low, medium, and high intensity, corresponding to approximately 25, 50, and 75%.

The "supply" treatment was intended to improve the functioning of markets by providing

[1]Department of Economics, University of Maryland, College Park, MD 20742, USA. [2]School of Management, Yale University, New Haven, CT 06520, USA.
*Corresponding author. E-mail: ahmed.mobarak@yale.edu